RSC Advances

PAPER

Physical properties of a Eu^{3+}-doped Zn$_2$SiO$_4$ phosphor ceramic material with enhanced thermal sensitivity at low temperatures

M. N. Bessadok, [iD] *[a] A. Bouri,[a] D. Ananias,[b] S. Mrabet,[a] C. Vázquez-Vázquez[c] and L. El Mir[a]

In the present study, a SiO$_2$/Zn$_2$SiO$_4$:Eu glass−ceramic composite was synthesized by a homemade modified sol−gel method. Structural, morphological, and optical properties were investigated. Structural and morphological analysis proves the existence of silica and zinc silicate phases with the latter surrounded and shielded by the silica matrix. Optical−vibrational analysis shows the fingerprint peaks of a Zn$_2$SiO$_4$ material, confirming the good establishment of the phase. Photoluminescence plots reveal the presence of strong Eu^{3+} ion emission lines that come from radiative recombination from $^5D_0$ to ^7F_J ($J = 0$–4) inner states. The curves prove, as well, the appearance of weak wide blue (450 nm) and green (530 nm) bands related, respectively, to oxygen deficiency and zinc vacancy emission centers related to silica/zinc silicate intrinsic defects. The latter are taken as a starting point to investigate the thermometry properties of the sample by combining them with the europium principal emission lines ($^7F_{1,2}$) to get a maximum relative sensitivity of 2.36% K^{-1} at the [12–140 K] temperature range. The findings are promising and show, for the first time, the thermometry study of Eu-doped zinc silicate at below room temperature range.

1. Introduction

In the previous few years, research groups have been concentrating on developing several materials with different properties allowing using them in multifunctional optics.[1–6] Among them, phosphor materials are taking nowadays an important place in the optoelectronics industry. Phosphors consist of a wide bandgap transparent host such as sulfates, vanadates, and silicates,[7–9] with metal ion centers embedded that can emit in the whole ultra violet-visible-near infrared (UV-vis-NIR) spectral range, after being exposed to different excitation energy sources like photons, thermal heating, and voltage.[10–12] As a result, the emitted light will be employed in display devices, cathode ray tubes, emitting diodes, and many other applications.[13] Among a large number of phosphor materials, zinc silicate (Zn$_2$SiO$_4$), known for its mineral name "willemite", stands as one of the oldest inorganic silicate-based materials that have high luminescence efficiency and good chemical stability.[14] This latter

feature is making it a good system at higher temperatures, maintaining very good luminescence properties. In addition, the environmental sustainability, affordable manufacturing and effective ultra-violet radiation absorption make it a desirable choice for versatile applications. Zinc silicate is a mineral system included in phenakite-type materials (Be$_2$SiO$_4$). The α-phase is known to be the most stable in the wide thermal region up to 1500 °C and belongs to trigonal $R3m$ space group.[15] However, the β-phase forms typically before 800 °C under specific circumstances, and then makes a phase transition to α-one before it reappears at about 1500 °C, but in a very narrow thermal region because of the fusion of the crystal at 1512 °C.[16] Until now, there is no precise refinement of the crystal lattice of β-phase. But most probably, it belongs to the triclinic or orthorhombic system. Moreover, zinc silicate is recognized as a wide bandgap material (~5.5 eV). The valence band is mainly made up of a mixture of 2p orbitals of oxygen alongside zinc's 4s, 4p and 3d ones, while the conduction band contains essentially zinc's 4s and 4p orbitals, silicon's 3p orbitals, and oxygen's 2p orbitals.[17] Such a wide bandgap system is similar to those of dielectric materials rendering it a very promising candidate in electric insulator applications.[18]

For a long time, research groups have been competing to produce zinc silicate (ZS) material by combining zinc oxide (ZnO) with glassy silicon dioxide (SiO$_2$) at a high annealing temperature above 700 °C. Numerous synthesis methods have in common to optimize the raw precursor quantities and reduce

*[a]Laboratory of Physics of Materials and Nanomaterials Applied at Environment (LaPhyMNE-LR05ES14), Faculty of Sciences in Gabes, Gabes University, 6072 Gabes, Tunisia. E-mail: mednafti.bessadok@fsg.rnu.tn

[b]Department of Chemistry, CICECO – Aveiro Institute of Materials, University of Aveiro, 3810-193 Aveiro, Portugal

[c]Laboratory of Magnetism and Nanotechnology (NANOMAG), Department of Physical Chemistry, Institute of Materials (iMATUS), Universidade de Santiago de Compostela, 15782 Santiago de Compostela, Spain*

the energy loss. Several optimized synthesis methods are reported, such as the conventional solid-state reaction method,[15,19] the sol–gel method,[20,21] the hydrothermal route,[22,23] the gel combustion process,[24] the polymer thermal treatment method[25] and many others. The diversity of synthesis routes coupled to the optimized experimental parameters and the adequate quantity of introduced impurities are helping to generate tunable properties that lead to many potential applications, such as optoelectronic devices,[26] photocatalytic activity,[27] high-frequency devices,[28] and mechanical tools.[17] However, despite the multifunctional aspect of willemite material, researchers are focusing principally on its luminescence properties and their applications. For instance, tremendous attention has been dedicated, especially to the Mn-activated ZS lattice,[29–32] which emits a strong and highly efficient green-yellow light that comes from the d–d transition of the Mn^{2+} ion. In addition, many other transition metals $(TM)^{[33,34]}$ and lanthanide $(Ln)^{[20,35,36]}$ activated ZS crystals are reported which proves the high applicability of such phosphor materials in several phosphors-based devices.

In the last 20 years, the contactless thermometry application has gained a lot of attention since it provides a simple way for temperature measurement, especially after the fast expansion of the COVID-19 pandemic. The temperature sensing can be operated in a wide temperature range[37,38] with quick response and high accuracy living cells millimeter-scale sensing. The developed method is a facile process of measuring temperature using simple tools based on the behavior of spatial and temporal parameters, which change dramatically with temperature variation.[39] Several parameters can be deduced from one temperature-dependent luminescence plot, which leads to the investigation of the potential use of a phosphor in thermometry applications. The most widespread parameter is the luminescence-integrated intensity since it is the simplest to measure. Researchers have used phosphors with one strong emission band such as the case of K. Kniec *et al.*[40] for vanadium-doped $Y_3Al_{5-x}Ga_xO_{12}$ and N. Saxena and her team for SiO_2–CdS nanocomposite material.[41] Despite its simplicity, one single emission band is highly sensitive to disturbance with moderate precision. The method can be easily affected by experimental factors such as the instability of the light source and the detectors, the absorption and scattering induced by the medium and the lack of an accurate calibration. Consequently, these issues may all cause a huge distortion and noise to the signal, leading to several measurement errors. Then, this method become almost ruled out in the current publications. However, the use of such approach is still very effective for activation energy calculation using the Boltzmann/Arrhenius models to reveal the required energy needed by one charge carrier in semiconductor systems. On the other hand, studies have been driven toward luminescence intensity ratio (LIR), which is one of the most used readout schemes that consists of combining two different emission bands and calculating their ratio pattern *versus* temperature. The method offers very good stability toward the excitation source fluctuations and provides a self-referencing character to the sensor. LIR method has been widely employed for doped and co-doped Ln-based

materials,[42,43] TM-based materials,[44] and TM/Ln co-doped materials such as the case of manganese/europium-activated $Y_3Al_5O_{12}$ crystal.[45] Another aspect of the LIR route is combining two bands with different behaviors; one with non or weak temperature trend and the second has a strong emission variation with temperature which is the case of several reports such as europium-doped TiO_2.[46] Recently, A. Ćirić and his co-workers developed, a new methodology based on the squared emission intensity applied to several phosphor materials.[47] The readout method consists of studying the overlapped emission bands; sharp first one and broad second one, which is mainly the case of chromium(III) and manganese(IV) ions. K. Trejgis and his team studied the emission behavior of one single emission band of Nd-doped NYF_4 phosphor[12] by calculating the LIR parameter of the same emission band that changes its profile by the use of two different excitation wavelengths. I. E. Kolesnikov *et al.*[48] have made a step further for the LIR method development by using the dual-mode excitation spectra for europium-doped $LaVO_4$. The method has been applied for a very large temperature range (98 to 773 K) by employing two different excitation sources and investigating their temperature trend. Alongside the intensity emission, several parameters were developed to get a better sensitivity for the temperature sensor. Spectroscopic parameters such as time decay,[37] band spectral broadening,[49] band shift,[50] Raman photoluminescence intensity ratio,[51] and many others[52–54] were all used for the development of new optical thermometry perspectives. However, even with the various readout schemes available, the luminescence intensity-based approach and its alternatives are still the most employed ones in actual literature reports, thanks to their simple instrumentations and very short processing time. On the other hand, other methods such as bandwidth and band shift offer much higher precision but generally require significant variation so that an accurate temperature can be detected, which is not the case in the majority of literature reports.

Among the different optical thermometry-based phosphor materials, the literature reviews have poorly dealt with the ZS crystal lattice. It can be noticed as well that all of the published papers have, only, focused on manganese-doped zinc silicate material (ZSM). V. Lojpur *et al.*[55] were the first to prove the potential use of such material in contactless thermometry by investigating the LIR parameter between the well-known strong green emission band and the non-temperature dependent lattice defects in the [303–573 K] thermal range. A similar approach has been utilized recently by M. N. Bessadok *et al.*[56] Therefore, Huang *et al.*[57] have employed the LIR scheme by combining europium-doped Gd_2O_3 with ZSM material to enhance the performance of the obtained phosphor-based sensor. L. El Mir[58] as well as K. Omri *et al.*[59] have studied the time decay of the ZSM sample in the [77–300 K] range and shown promising results. Luminescence lifetime decay is a very attractive readout method since it is unaffected by external electromagnetic field interference and the inhomogeneity of the light fields. However, it always needs a quite higher processing time and complex instrumental setup.

In order to improve the performance of zinc silicate-based optical thermometer, doping with high emitting ions such as

lanthanide elements is a wise approach. Among the numerous lanthanides, europium stands as one of the most utilized ones thanks to its bright and high color purity red emission bands. While other lanthanide elements such as terbium (Tb^{3+}), neodymium (Nd^{3+}) and dysprosium (Dy^{3+}) possess tremendous optical properties, trivalent europium has its own unique features such as a higher quantum efficiency alongside superior stability. Furthermore, europium is much more abundant in Earth's crust compared to other lanthanide elements that are less easily extracted and/or remarkably more expensive. In addition, the use of europium is primarily specialized to displays and optical technologies, while other lanthanide elements being used in broader fields such as batteries and magnets. Hence, europium become more favorable choice than other lanthanide elements to develop the thermometric properties of materials.

Herein, we present in the current paper the thermometry properties of europium(III)-doped Zn_2SiO_4 material, carried out at very low temperatures. Despite the numerous papers dealing with Eu^{3+} activated ZS material,[60–64] we cannot find any temperature dependence study nor luminescence thermometry investigation of the sample. For that, we propose in the present study to look into the structural, morphological, vibrational, and optical properties of the Eu-doped zinc silicate sample. The optical thermometry study has been fulfilled as well for the first time. The obtained results from the luminescence study prove the great potential to explore such a ceramic composite material in optoelectronic devices. More importantly, the good sensitivity value in the cryogenic temperature range (typically below 120 K) serves for temperature measurement in a broad range with quite high accuracy. The use of Eu-activated zinc silicate for optical thermometry is crucial since it enables local temperature measurement in hostile conditions with limited access. Such measurement is done in a contactless way that does not interfere with the system and maintains its stability toward perturbations, so that we obtain an accurate temperature measurement. As a result, it can be employed for low-temperature systems such as superconducting materials and superfluid helium (He II).

2. Material and method

One of the novelties of this work is the use of multi-step homemade protocol. Previously, our laboratory team group have successfully produced several metal doped zinc silicate through the same procedure, that exhibits excellent luminescence properties.[21,65,66] We suggest here the employment of such protocol to elaborate lanthanide-activated zinc silicate material. In this process, Eu-doped Zn_2SiO_4 aerogel material embedded in a silica glass matrix was fabricated through a modified sol–gel method using supercritical conditions of ethanol in a stainless-steel autoclave. First, nanoparticles of Eu1%-doped ZnO (EZO) were synthesized in such a way that $[Eu]/[Zn] = 0.01$ using zinc acetate dihydrate ($Zn(CH_3COO)_2 \cdot 2H_2O$, 99%, Sigma-Aldrich) and europium(III) acetate hydrate ($Eu(CH_3CO_2)_3 \cdot xH_2O$, 99.9%, Sigma-Aldrich). Then, tetraethylorthosilicate (TEOS) ($C_8H_{20}O_4Si$, 98%, Sigma-Aldrich) was employed to get $SiO_2/$

ZnO:Eu1% composite at a maximum temperature of 250 °C. At this stage, ZnO grains are incorporated into the porous silica body, where Zn and Si species are quite close. Finally, the composite will be heated at 1200 °C for 2 hours to transform it into SiO_2/Zn_2SiO_4:Eu1% (EZS) glass–ceramic material using a solid-state reaction. Since Zn and Si atoms are quite close, the reaction will be much easier, which creates a smaller grain compared to the classic solid-state methods that produce a large micrometer grain at high annealing temperatures. More details about the synthesis method can be found in our previous work.[65] Room temperature structural, morphological and optical–vibrational properties were studied by a PANalytical diffractometer ($\lambda = 1.540598$ Å), HD2700 Hitachi scanning-transmission electron microscope (STEM), equipped with mapping element imaging, JASCO FT-IR 4X spectrometer and a WITec ALPHA300R+ confocal Raman microscope equipped with a 488 nm excitation laser. Room and low-temperature photoluminescence properties are investigated through a Fluorolog-3 Horiba spectrophotometer coupled to an R928 Hamamatsu photomultiplier with a 450 W Xe arc lamp for excitation.

3. Results and discussion

3.1. Eu-doped ZnO characterization

Fig. 1 shows the different characterizations of the EZO sample. X-ray diffraction (XRD) pattern proves the good establishment of the hexagonal-wurtzite structure of ZnO nanoparticles, supported also by a hexagonal shape like in the transmission electron microscope (TEM) image. In addition, we note the appearance of the characteristic peaks of ZnO crystal lattice in both Fourier transformation infrared (FTIR) and Raman spectra, which is in very good agreement with the literature.[67,68] From the obtained data, we can confirm the successful synthesis of EZO nanoparticles, which will be the starting point for studying the properties of SiO_2/EZS composite material.

3.2. Structural, morphological and vibrational properties of Eu-doped Zn_2SiO_4

Fig. 2(a) and (b) show the XRD pattern of SiO_2/EZS composite material. Well-crystallized peaks related to silica and zinc silicate are shown with silica being crystallized into a cristobalite allotropic phase (JCPDS card no. 01-071-0785). In many studies related to zinc silicate material, researchers are reporting a pure ZS phase with no impurities or secondary phase, which is related to the used protocol in which they have a total vanishing of silica phase.[20,33] On the other hand, this is not the case in our study since silica is present in excess and plays a crucial role as a matrix; a protector of zinc silicate grains from the outside environment. In addition, we have performed an optical–vibrational study through FTIR and Raman analysis. The transmitted infrared light curve (Fig. 2(c)) demonstrates the presence of ZnO_4 (619 cm^{-1}) and SiO_4 (870, 906, 933 and 975 cm^{-1}) absorption bonds. These tetrahedrons are the main components of the zinc silicate structure. A periodic lattice of ZnO_4 and SiO_4 tetrahedrons composes a Zn_2SiO_4 structure with one shared oxygen atom in the middle. More discussions about
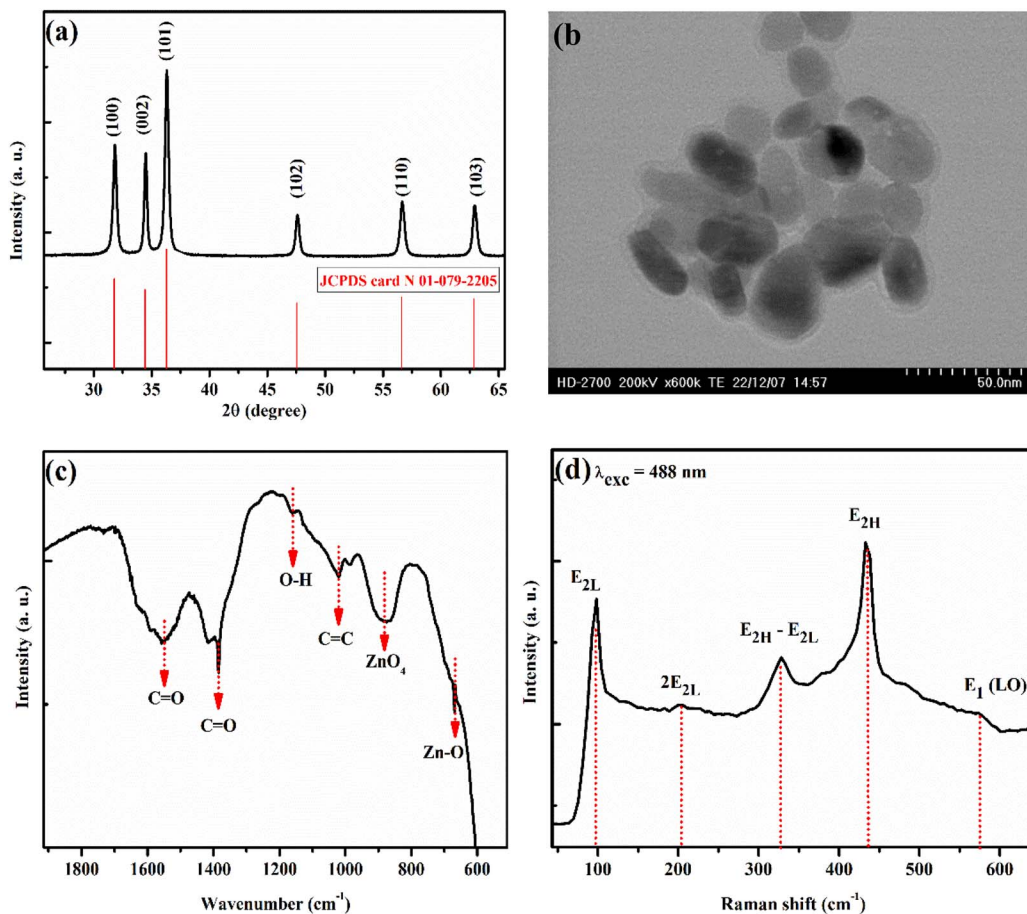
Fig. 1 Different room temperature characterizations of EZO sample. (a) XRD diffractogram. (b) TEM image. (c) FTIR transmitted light curve. (d) Raman spectrum recorded at 488 nm excitation wavelength.

the crystalline structure of zinc silicate material are nicely described in the work of T. I. Krasnenko and her team.[15] In addition, we show the existence of siloxane (Si–O–Si) active modes in the Raman spectrum reported at 874, 910, and 954 cm^{-1} (Fig. 2(d)). The obtained results are in very good agreement with the literature[11,19] and come to confirm the XRD results that prove the good establishment of the zinc silicate phase.

Moreover, the microstructure of the sample has been investigated through the STEM technique (Fig. 3) which shows a micrometer-sized body related to the silica phase that acts as a coater of zinc silicate's grain. The mapping analysis images (different atoms as labelled by different colors; green for oxygen, blue for zinc, red for silicon and cyan for europium) prove a typical core/shell structure of the SiO$_2$/ZS system. The observed morphology is a direct consequence of the utilized homemade protocol and it presents a similar result compared to the case of manganese-doped ZS crystal, studied previously by our laboratory team.[69] It can be said that these features encouraged us to investigate the photoluminescence properties of the samples. In reality, luminescence properties are directly enhanced by the presence of a core–shell morphology, since the shell will reduce the non-radiative surface defects, stabilize the internal core as well as enhance the luminescence thermometry sensitivity.[70–72]

In summary, the developed home-made protocol presents a powerful synthesis procedure for implanting phosphors materials into silica porous matrix body. Such procedure has a big advantage in term of dispersing the grains into the matrix. The closeness of Zn, Si and O atoms into the structure help to obtain the desired phase in a much simpler way while keeping a smaller size than conventional solid-state methods. A very good homogeneity and dispersion of the grains is obtained, that will enhance the photoluminescence properties of the samples.

3.3. Photoluminescence investigation of Eu-doped Zn$_2$SiO$_4$

Room temperature photoluminescence (PL) emission curve of EZS material (Fig. 4(a)) depict typical emission lines of Eu^{3+} ions related to the well-known $^5D_0$–^7F_J transitions. The red emission peaks are located at 577, 591, 610, 652, and 703 corresponding to J = 0–4 respectively. The same graph shows the room temperature photoluminescence excitation spectrum (PLE) which reveals typical absorption bands arising from an efficient charge transfer from $^7F_0$ and $^7F_1$ states. Fig. 4(b) shows an extra green broad emission band related to zinc silicate intrinsic
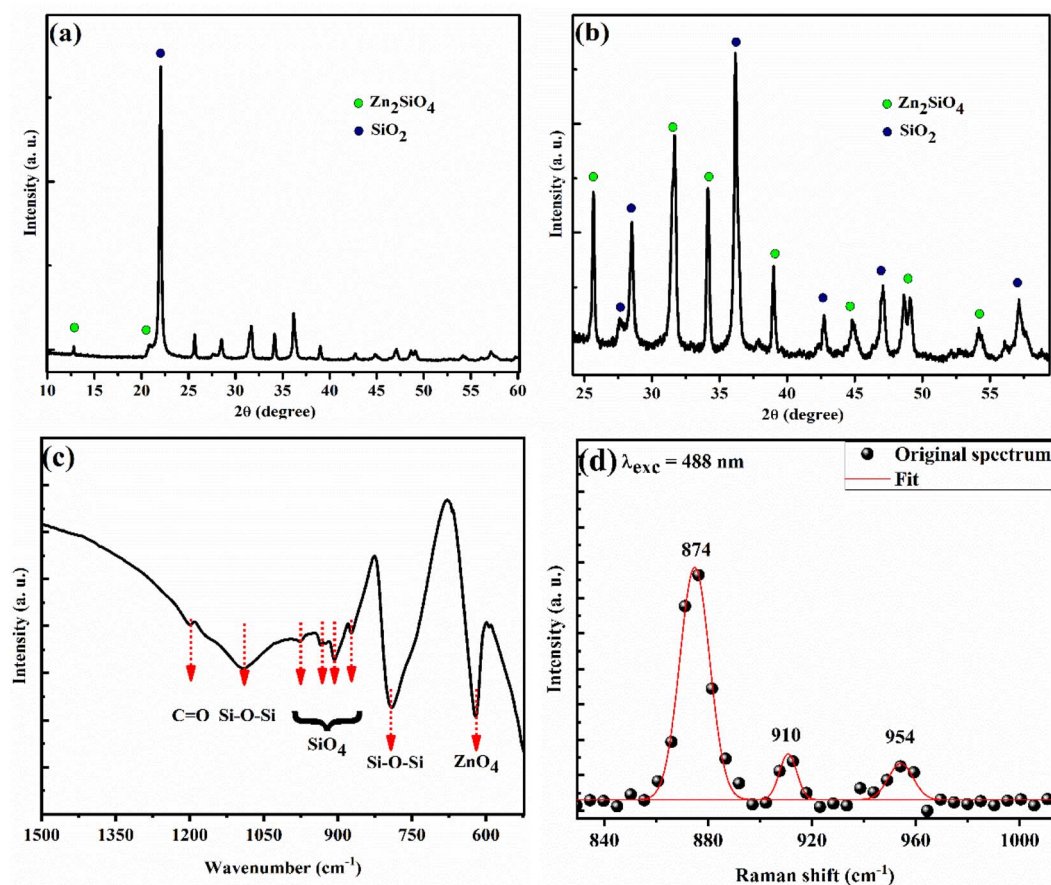
Fig. 2 Different characterizations of the EZS sample. (a) XRD diffractogram with different labels corresponding to silica and zinc silicate phases. (b) A close look into [23–60°] angular range of XRD graph. (c) FTIR transmitted light curve. (d) Raman spectrum recorded at 488 nm excitation wavelength.

defects. Y. Sun et al.[73] have studied the defects emission into zinc silicate lattice. In their paper, the authors mentioned that such a green band arises essentially from zinc vacancy defects (V_{Zn}), which come from the stoichiometric ratio deficiency of zinc atoms and the effect of high annealing temperature. In addition, such emission seems to persist in the whole [12–300 K] range with a weak temperature dependence character (onset Fig. 4(c)). Besides, a broad blue emission appears around 450 nm which seems to disappear beyond 180 K. I. M. Alibe et al.[74] have studied the room temperature PL emission of pure ZS material and reported a sharp weak blue emission at around 447 nm, they explain that emission is arising from oxygen defects. P. Diana and her co-workers have reported a similar band (~463 nm) at room temperature, which enhances a lot by raising the calcination temperature from 800 to 1200 °C, without identifying its true origin. For our case, we propose that such a band comes from silica's lattice oxygen-native defects. Such attribution is sustained by the fact that the SiO_2 lattice is rich in several visible-emitted centers related to oxygen defects arising from the different experimental conditions as reported earlier.[75,76] More particularly, we propose that the blue emission band is related to the intrinsic defects called oxygen deficiency centers-type II (ODC II), which are created in irradiated glasses

and present two-fold coordinated silicon centers (=Si⋯) that are responsible, generally, for the emission band around [440–460 nm].[77] This is supported as well by the double absorption bands at 274 and 282 nm (onset Fig. 4(d)) that are similar to the case of the Si–SiO_2 thin layers system (~269 nm) which contributed to the blue emission (~450 nm) as reported by A. P. Baraban et al.[78] Additionally, the PLE spectra show a strong Eu–O charge transfer band (CTB) around 240 nm. It can be speculated, also, that such a band can be attributed to the non-bridging oxygen hole center (NBOHC) which is a typical silica defect that absorbs energy at around 4.8 eV (258 nm). The overlapping of both absorption bands is still possible and cannot be ruled out.

In conclusion, since europium ion has a different oxidation state (+III) than zinc's (+II), some crystal defects will be created in order to balance the charge deficiency. This is supported, as well, by the use of multi-steps elaboration method coupled to the high annealing temperature, leading to an increased amount of zinc and oxygen defects. These imperfections are characterized by different emission centers positioned in the bandgap of zinc silicate material, and they are populated through an effective energy transfer from the high absorption band at 5.16 eV (240 nm). Hence, the population of such centers
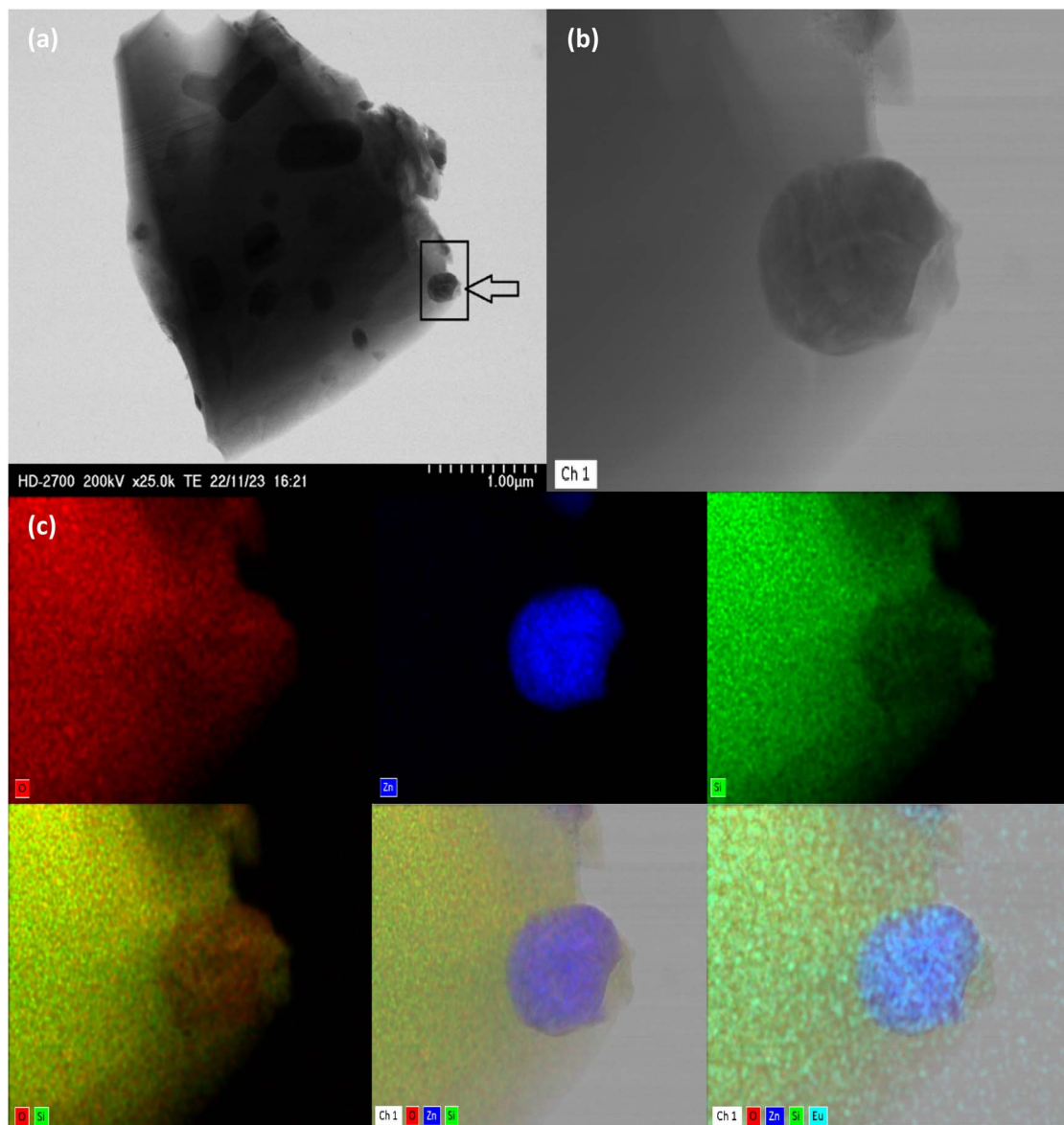
Fig. 3 Morphology of SiO_2/Zn_2SiO_4:Eu through TEM setup. (a) SiO_2/EZS composite. (b) Zoom of the mentioned frame. (c) Mapping element analysis of (b).

will generate the blue/green emission followed by the charge carrier recombination to the valence band. Such bands have a very weak temperature dependency which presents a solid point to base on in thermometry study.

3.4. Luminescence thermometry study

We have clearly shown in Fig. 4(c) that the EZS sample can emit in the whole [12–300 K] range with an intensity quenching effect by the measurement temperature increment. This feature is a good starting point to explore the luminescence thermometry properties of the sample. The performances of phosphor-based sensors can be examined by calculating the relative sensitivity given in percentage per kelvin (% K^{-1}) that, generally, surpasses ~1% K^{-1} for good temperature sensors. In most LIR studies, researchers are using coupled levels from doped Ln-based

phosphors. In general, the thermal levels coupling takes place by using two adjacent energy states obeying to Boltzmann distribution law (LIR ~ $\exp(\Delta E/k_B T)$) with an energy gap lower than 2000 cm^{-1}. This limitation helps avoid the decoupling process which makes the temperature effect much less predominant for the energy transfer process between overlapped states. Nevertheless, that limitation will lead to a maximum value of the relative sensitivity that cannot be surpassed ($S_r = \Delta E/k_B T^2$). This restriction makes the use of the sensor, less important in several applications. That is why, to overcome the issue, researchers are taking into consideration other ways such as non-thermally coupled levels coming from different Ln ions (such as the case of Tb^{3+}/Eu^{3+} and Yb^{3+}/Er^{3+} ref. (79)) and the emission centers from the host intrinsic deep defects. In our case, we considered four different LIR parameters by combining the deep host emissions (blue one at 450 nm
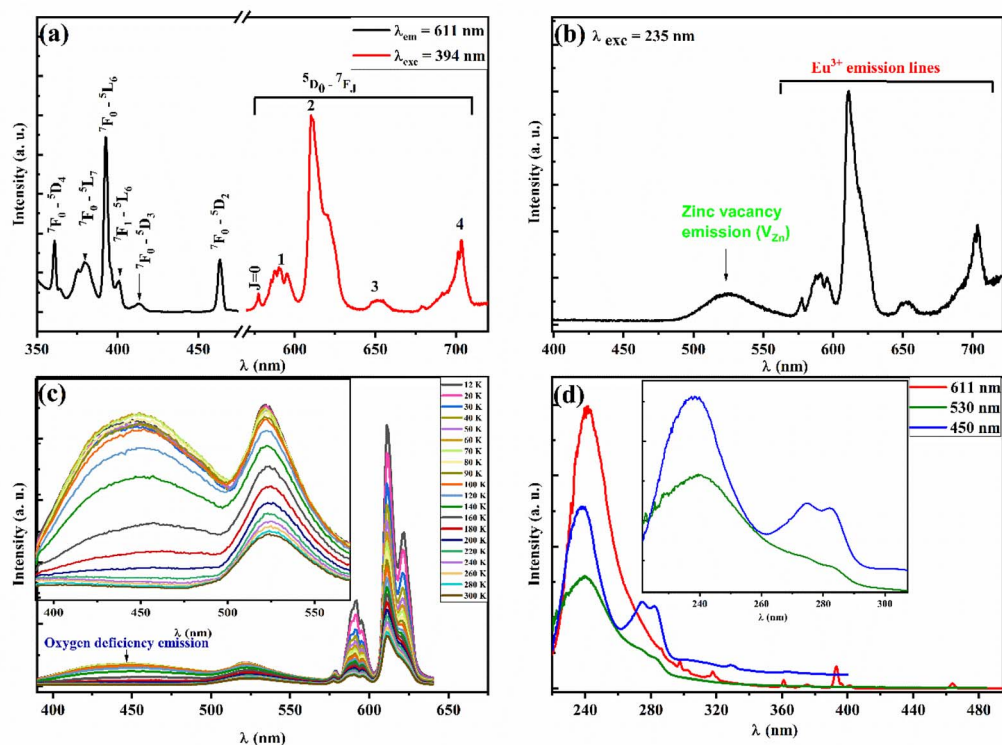
Fig. 4 (a) Typical absorption and emission spectra of EZS sample at room temperature. (b) Emission spectrum at 235 nm excitation wavelength. (c) Emission spectra of EZS sample at 240 nm excitation wavelength for the whole [12–300 K] temperature range. The onset shows a close look into the [400–560 nm] spectral range. (d) PLE spectra at 12 K for the different emissions. The onset shows a close look into the blue and green emissions absorption bands.

and green at 530 nm) with the europium's strongest emission lines ($^7F_1$ at 591 nm and $^7F_2$ at 611 nm). The different LIR parameters are defined as follows (by referring to intensity):

$$LIR_1 = \frac{I_{450}}{I_{591}}; \; LIR_2 = \frac{I_{450}}{I_{611}}; \; LIR_3 = \frac{I_{530}}{I_{591}}; \; LIR_4 = \frac{I_{530}}{I_{611}}.$$

The europium lines are highly temperature-depending parameters while the host deep defects have a weekly temperature dependence character. This latter is the key factor in the new LIR methods, in which the ratio is calculated based on a weekly or non-temperature dependent emission band so that the second line cannot be affected by measurement errors like those coming from excitation source fluctuation, the inhomogeneity of the nano-phosphor or the instabilities in the detection. This method brings a lower sensitivity to disturbance, higher reliability and faster response. All the 4 LIR curves are presented in Fig. 5 with the suitable fitting parameters summarized in Table 1 corresponding to a 3rd order polynomial function ($LIR = A_0 + A_1 T + A_2 T^2 + A_3 T^3$), which has been widely employed[37,80–83] despite not being a widespread model compared to the Boltzmann and/or Arrhenius-like fit equation models. It is worth mentioning that in some cases, the LIR value will be similar at two different temperature values, which restricts its applicability in optical thermometry. That is why the fitting line as well as the operating temperature range will be limited to [12–120 K] for LIR (1–2) and to [12–140 K] for LIR (3–4) parameters.
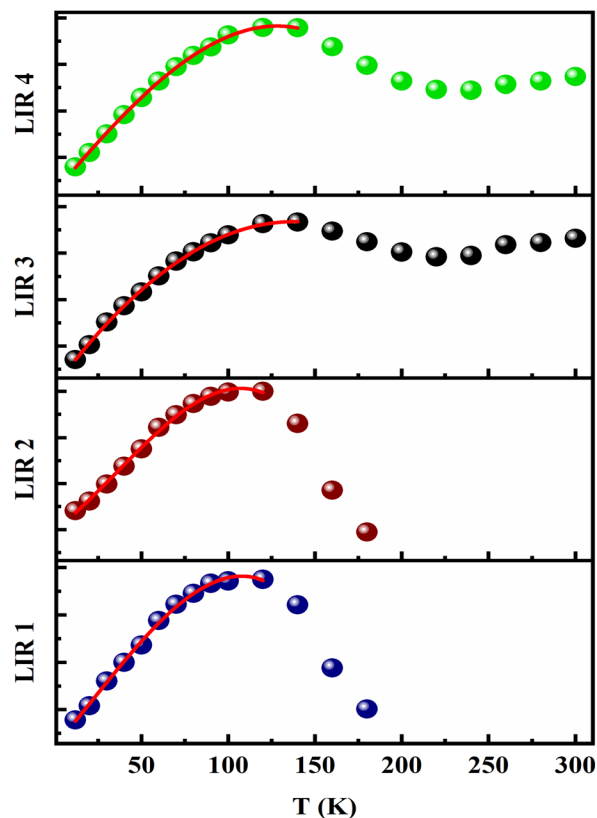

Fig. 5 Temperature evolution for LIR_{1-4} parameters. The entire patterns are fitted with 3rd order polynomial function.

Table 1 Fitting adjustment parameters of the 3rd order polynomial LIRs curves

|	LIR 1	LIR 2	LIR 3	LIR 4
A_0	0.17227	0.06752	0.17936	0.07202
A_1	0.00594	9.76178×10^{-4}	0.00805	0.00143
A_2	1.95698×10^{-5}	9.19241×10^{-6}	-2.70114×10^{-5}	-1.34763×10^{-6}
A_3	-2.92278×10^{-7}	-8.56441×10^{-8}	-1.06873×10^{-8}	-2.19279×10^{-8}
R^2 adjusting coefficient	0.9975	0.9970	0.9991	0.9994

As reported before, the relative sensitivity is one of the best parameters to base on in luminescence thermometry theory since it shows the potential use of the phosphor materials as a practical contactless thermometer in different temperature ranges. It describes also the performances and allows them to compare the several sensors. The relative sensitivity is given generally by the following equation:

$$S_r = \left| \frac{100\%}{LIR} \frac{dLIR}{dT} \right| \qquad (1)$$

The S_r curves corresponding to the different ratios are presented in Fig. 6. The reported maximum sensitivity values are 2.14, 1.27, 2.36, and 1.37% K^{-1} for LIR_{1-4} respectively. The obtained values are quite good compared to the earlier reports dealing with Eu^{3+}-single doped phosphor material using the LIR technique (Table 2). It is noteworthy as well that most studies are dealing with high-temperature range values above

room temperature (>300 K). In addition, to the best of our knowledge, this is the first report dealing with the thermometry properties of Eu-doped zinc silicate material at low temperatures.

To sum up, to the best of our knowledge, this is the first attempt to uncover the potential use of Eu-doped Zn_2SiO_4 in the optical thermometry research field. Indeed, the LIR method has gained popularity in the actual reports since it calculates the intensity ratio between two different dopant elements or more that are easily measured in current optical devices. Actually, such procedure is simpler to use and lead to tremendous relative sensitivity values across a broad operating temperature range.[9] Nevertheless, co-doping with another lanthanide is more expensive due to the elevated cost of raw precursors. That is why merging one single lanthanide element's emission bands with intrinsic host defects remains an effective low-cost approach. Such procedure requires always the use of the suitable host lattice in which the effect of the intrinsic defect is
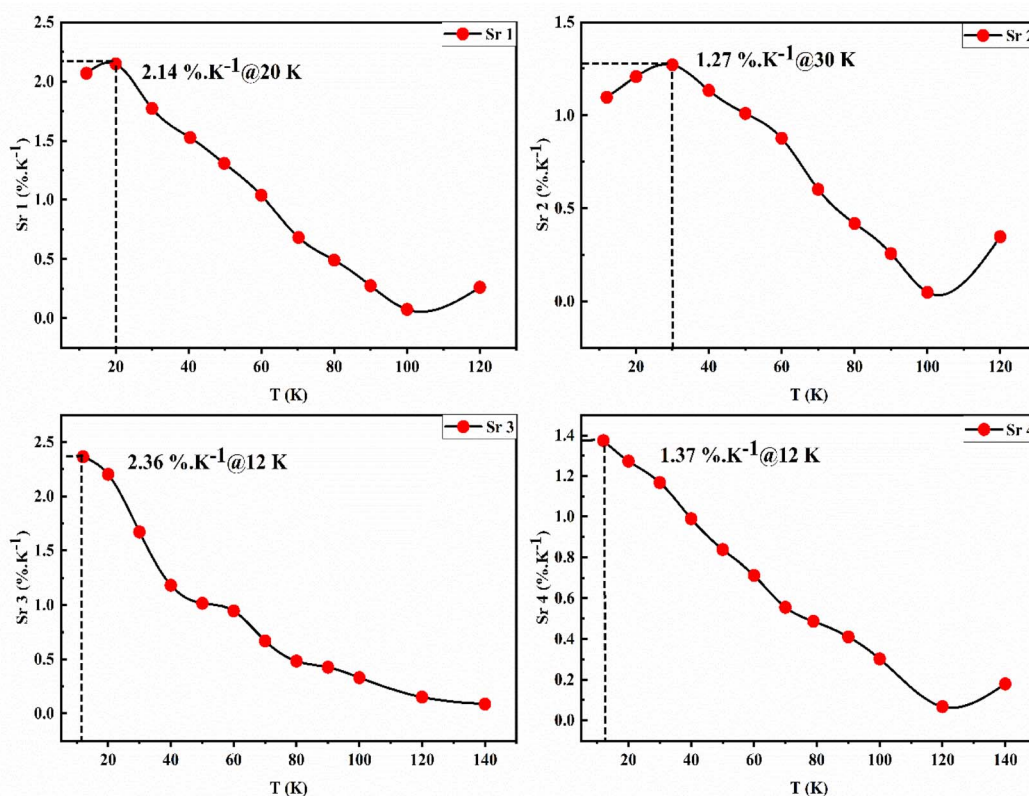
Fig. 6 Pattern of relative sensitivity (Sr_{1-4}) *versus* temperature.

Table 2 Comparison between different sensitivity values reported in the literature, which obtained from single Eu^{3+}-doped host materials. The given values of S_r concern, only, those using the intensity ratio technique between one host defect emission band and one europium emission line

Material	Optical readout scheme	S_r (% K^{-1})	Operating temperature range (K)	References
Zn$_2$SiO$_4$:Eu 1%	LIR	2.14	12–120	Current study
		1.27		
		2.36	12–140	
		1.37		
SrZrO$_3$:Eu 2%	LIR	2.22	300–550	84
LiCa$_3$ZnV$_3$O$_{12}$:Eu 0.75%	LIR	1.18	303–483	85
LiCa$_3$MgV$_3$O$_{12}$:Eu 0.25%	LIR	1.69	303–523	86
Ba$_3$La(VO$_4$)$_3$:Eu 0.01%	LIR	1.77	298–573	87
YVO$_4$:Eu 0.1%	LIR	1.38	123–323	88
Na$_3$Y(VO$_4$)$_2$:Eu 15%	LIR	2.70	298–440	8
TiO$_2$:Eu 3%	LIR	2.43	307–533	46

significant. In this regard, the sol–gel method is still a rapid and inexpensive synthesis procedure for obtaining a ternary silicate-based system that shows such intrinsic defect with appreciable thermal behavior. Moreover, zinc silicate has a less complex lattice than certain vanadate-based materials commonly used for optical thermometry (Table 2) as well as some other advanced systems, such as perovskites[43] and garnet-structured materials.[89] In addition, it must be said that despite the fast expansion of optical thermometry methods, this field still immature since it needs a further development to eliminate some theoretical and methodological issues. In that sense, it must be in mind that the performance of any sensor is a combination of the used phosphors materials, readout scheme and the theoretical fit-model employed since there is no unique model for LIR data fitting. That is why; efforts are driven towards finding new optical active host materials with innovative readout schemes and methods for data analysis fitting, and even re-investigating the old ones to correct some common errors in calculations.

4. Conclusion

In the present work, we have successfully produced zinc silicate phosphor material embedded into a silica host matrix. The employed protocol developed by our lab team presents a simple tool to get an homogeneous structure with good physical properties. XRD and TEM analysis prove the successful establishment of the desired phase with zinc silicate grains shielded by the host matrix that helps to reduce surface defects and enhance the optical properties. FTIR and Raman analysis support the successful synthesis of the sample and show the presence of zinc silicate fingerprint peaks (SiO$_4$, ZnO$_4$, and Si–O–Si bonds). Doping with europium helps to enhance the optical properties of the sample, which presents fine sharp red emission lines with two broad bands at blue and green spectral regions (450 nm and 530 nm respectively). The low-temperature measurement study is helping to investigate the luminescence thermometry properties of Eu-doped zinc silicate. Four different LIR parameters were studied to show the

potential use of such crystal material in optical thermometry. A maximum sensitivity value of about 2.36% K^{-1} is obtained when combining the broad green emission with the $^7F_1$ emission line. Despite the good reported values, some additional investigations are required to enhance to performance of the sensor and expand the operating temperature range using a second Ln/TM activator. The different incorporated ions are inducing several orbitals overlap into the coordinate energy diagram, which facilitates the charge transfer process between the various states. Therefore, it contributes significantly to the elevation of sensitivity value and enlarging the operating range temperature.

Data availability

The authors confirm that the data used to support the findings of this study are included within the article and are available from the corresponding author upon reasonable request.

Author contributions

M. N. Bessadok: conceptualization, methodology, investigation, writing – original draft, visualization. A. Bouri: conceptualization, investigation. D. Ananias: conceptualization, investigation, resources. S. Mrabet: investigation, resources. C. Vázquez-Vázquez: investigation, resources. L. El Mir: conceptualization, methodology, resources, writing – review & editing.

Conflicts of interest

The authors declare no conflict of interest.

Acknowledgements

References

1 B. Tiss, D. Martínez-martínez, B. Silva, N. Bouguila, L. El Mir, B. Almeida, C. Moura and L. Cunha, *Opt. Laser Technol.*, 2024, **174**, 110673.

2 W. Ahmed, L. Chouiref, H. Dahman, L. El Mir and H. L. Gomes, *Appl. Sci.*, 2023, **13**, 1069.

3 O. Amorri, H. Slimi, A. Oueslati, A. Aydi and K. Khirouni, *Phys. B*, 2022, **639**, 414005.

4 M. Benamara, N. Zahmouli, A. Kallekh, S. Bouzidi, L. El Mir, H. R. Alamri and M. Almeida Valente, *J. Magn. Magn. Mater.*, 2023, **569**, 170479.

5 S. Mrabet, N. Ihzaz, M. Alshammari, N. Khlifi, M. Ba, M. N. Bessadok, I. H. Mejri and L. El Mir, *J. Alloys Compd.*, 2022, **920**, 165920.

6 D. Rahmatabadi, M. Aberoumand, K. Soltanmohammadi, E. Soleyman, I. Ghasemi, M. Baniassadi, K. Abrinia, M. Bodaghi and M. Baghani, *Adv. Eng. Mater.*, 2023, **25**, 2201309.

7 A. S. Messalti, M. El-Ghozzi, D. Zambon, R. Mahiou and Z. Setifi, *J. Lumin.*, 2021, **238**, 118227.

8 I. Kachou, K. Saidi, R. Salhi and M. Dammak, *RSC Adv.*, 2022, **12**, 7529–7539.

9 M. Sójka, W. Piotrowski, L. Marciniak and E. Zych, *J. Alloys Compd.*, 2024, **970**, 172662.

10 N. Khlifi, N. Ihzaz, S. Mrabet, A. Alyamani and L. El Mir, *J. Lumin.*, 2022, **245**, 118770.

11 P. Diana, S. Sebastian, D. Sivaganesh, C. S. A. Raj, S. S. Kumar Jacob, T. H. AlAbdulaal and M. Shkir, *Radiat. Phys. Chem.*, 2023, **212**, 111156.

12 K. Trejgis, K. Ledwa, L. Li and L. Marciniak, *J. Mater. Chem. C*, 2022, **10**, 3006–3014.

13 C. W. Mun, L. Z. Wei and M. H. M. Zaid, *J. Mol. Struct.*, 2022, **1248**, 131474.

14 M. Takesue, H. Hayashi and R. L. Smith, *Prog. Cryst. Growth Charact. Mater.*, 2009, **55**, 98–124.

15 T. I. Krasnenko, R. F. Samigullina, N. A. Zaitseva, I. I. Ivanova, S. V. Pryanichnikov and M. V. Rotermel, *J. Alloys Compd.*, 2022, **907**, 164433.

16 S. E. Elhadi, C. Liu, Z. Zhao, K. Li and X. Zhao, *Thin Solid Films*, 2018, **668**, 1–8.

17 R. Dai, R. Cheng, J. Wang, C. Zhang, C. Li, H. Wang, X. Wang and Y. Zhou, *J. Adv. Ceram.*, 2022, **11**, 1249–1262.

18 B. Synkiewicz-Musialska, D. Szwagierczak, J. Kulawik, N. Pałka and P. R. Bajurko, *J. Eur. Ceram. Soc.*, 2020, **40**, 362–370.

19 G. Essalah, G. Kadim, A. Jabar, R. Masrour, M. Ellouze, H. Guermazi and S. Guermazi, *Ceram. Int.*, 2020, **46**, 12656–12664.

20 P. Mbule, D. Mlotswa, B. Mothudi and M. Dhlamini, *J. Lumin.*, 2021, **235**, 118060.

21 K. Omri, A. Alyamani and L. El Mir, *Appl. Phys. A:Mater. Sci. Process.*, 2018, **124**, 1–7.

22 D. K. Bharti, K. Verma, A. K. Srivastava and M. K. Gupta, *J. Appl. Phys.*, 2020, **127**, 085104.

23 R. F. Samigullina, A. P. Tyutyunnik, I. N. Gracheva, T. I. Krasnenko, N. A. Zaitseva and T. A. Onufrieva, *Mater. Res. Bull.*, 2017, **87**, 27–33.

24 Z. G. Portakal-Uçar, M. Oglakci, M. Yüksel, M. Ayvacıklı and N. Can, *Mater. Res. Bull.*, 2021, **133**, 111025.

25 I. M. Alibe, K. A. Matori, M. H. M. Zaid, S. Nasir, A. M. Alibe and M. Z. A. Khiri, *Materials*, 2021, **14**, 1–26.

26 L. El Mir, *J. Mater. Sci.:Mater. Electron.*, 2018, **29**, 20493–20499.

27 N. Alonizan, L. Chouiref, K. Omri, M. A. Gondal, N. Madkhali, T. Ghrib and A. I. Alhassan, *J. Inorg. Organomet. Polym. Mater.*, 2020, **30**, 4372–4381.

28 K. Omri and R. Lahouli, *J. Mater. Sci.:Mater. Electron.*, 2019, **30**, 7834–7839.

29 T. Kang, H. Kang, S. Park, G. Deressa, J. Park and J. Kim, *Mater. Today Commun.*, 2021, **26**, 101798.

30 J. Park and J. Kim, *J. Alloys Compd.*, 2021, **855**, 157343.

31 K. Omri and F. Alharbi, *J. Mater. Sci.:Mater. Electron.*, 2021, **32**, 12466–12474.

32 M. M. Afandi, S. Byeon, T. Kang, H. Kang and J. Kim, *Nanomaterials*, 2024, **25**, 1395.

33 P. Diana, S. Sebastian, S. Saravanakumar, V. Ganesh and T. H. AlAbdulaal, *Opt. Mater.*, 2023, **138**, 113632.

34 J. El Ghoul, *J. Mater. Sci.:Mater. Electron.*, 2018, **29**, 2999–3005.

35 P. Vařák, P. Nekvindová, S. Vytykáčová, A. Michalcová, P. Malinský and J. Oswald, *J. Non-Cryst. Solids*, 2021, **557**, 120580.

36 A. Z. K. Azman, K. A. Matori, S. H. Ab Aziz, M. H. M. Zaid, S. A. A. Wahab and R. E. M. Khaidir, *J. Mater. Sci.:Mater. Electron.*, 2018, **29**, 19861–19866.

37 M. Sójka, M. Runowski, T. Zheng, A. Shyichuk, D. Kulesza, E. Zych and S. Lis, *J. Mater. Chem. C*, 2022, **10**, 1220–1227.

38 D. Yu, H. Li, D. Zhang, Q. Zhang, A. Meijerink and M. Suta, *Light:Sci. Appl.*, 2021, **10**, 4–15.

39 M. D. Dramićanin, *J. Appl. Phys.*, 2020, **128**, 040902.

40 K. Kniec, K. Ledwa and L. Marciniak, *Nanomaterials*, 2019, **9**, 1375.

41 N. Saxena, P. Kumar and V. Gupta, *RSC Adv.*, 2015, **5**, 73545–73551.

42 D. Ananias, F. A. Almeida Paz, L. D. Carlos and J. Rocha, *Chem.–Eur. J.*, 2018, **24**, 11926–11935.

43 H. Zhang, Z. Gao, G. Li, Y. Zhu, S. Liu, K. Li and Y. Liang, *Chem. Eng. J.*, 2020, **380**, 122491.

44 L. Marciniak, K. Kniec, K. Elżbieciak-Piecka, K. Trejgis, J. Stefanska and M. Dramićanin, *Coord. Chem. Rev.*, 2022, **469**, 214671.

45 J. Periša, V. Đorđević, Z. Ristić, M. Medić, S. Kuzman, Ž. Antić and M. D. Dramićanin, *Mater. Res. Bull.*, 2022, **149**, 111708.

46 M. G. Nikolić, Ž. Antić, S. Ćulubrk, J. M. Nedeljković and M. D. Dramićanin, *Sens. Actuators, B*, 2014, **201**, 46–50.

47 A. Ćirić, Ł. Marciniak and M. D. Dramićanin, *J. Appl. Phys.*, 2022, **131**, 114501.

48 I. E. Kolesnikov, D. V. Mamonova, M. A. Kurochkin, V. A. Medvedev and E. Y. Kolesnikov, *Ceram. Int.*, 2023, **49**, 20699–20705.

49 A. Ćirić, S. Stojadinović and M. D. Dramićanin, *Sens. Actuators, A*, 2019, **295**, 450–455.

50 L. Marciniak, A. Bednarkiewicz, D. Hreniak and W. Strek, *J. Mater. Chem. C*, 2016, **4**, 11284–11290.

51 A. De, V. Dwij, V. Sathe, M. A. Hernández-Rodríguez, L. D. Carlos and R. Ranjan, *Phys. B*, 2021, **626**, 413455.

52 J. Zhou, R. Lei, H. Wang, Y. Hua, D. Li, Q. Yang, D. Deng and S. Xu, *Nanophotonics*, 2019, **8**, 2347–2358.

53 L. Marciniak and K. Trejgis, *J. Mater. Chem. C*, 2018, **6**, 7092–7100.

54 Ž. Antić, A. Ćirić, M. Sekulić, J. Periša, B. Milićević, A. N. Alodhayb, T. A. Alrebdi and M. D. Dramićanin, *Crystals*, 2023, **13**, 884.

55 V. Lojpur, M. G. Nikolić, D. Jovanović, M. Medić, Ž. Antić and M. D. Dramićanin, *Appl. Phys. Lett.*, 2013, **103**, 2–5.

56 M. N. Bessadok, D. Ananias, A. Bouri, C. Bouzidi, C. Barthou and L. El Mir, *J. Lumin.*, 2024, **269**, 120480.

57 F. Huang and D. Chen, *J. Mater. Chem. C*, 2017, **5**, 5176–5182.

58 L. El Mir, *J. Inorg. Organomet. Polym. Mater.*, 2021, **31**, 2648–2653.

59 K. Omri and F. Alharbi, *J. Mater. Sci.:Mater. Electron.*, 2021, **32**, 24229–24239.

60 S. H. Jaafar, M. H. Mohd Zaid, K. A. Matori, Y. Yaakob and H. M. Mustapha, *Braz. J. Phys.*, 2022, **52**, 1–9.

61 K. N. Prathibha, R. H. Krishna, B. V. Nagesh, D. Prakashbabu, B. S. Panigrahi and R. Ananthanarayanan, *J. Mater. Sci.:Mater. Electron.*, 2021, **32**, 20197–20210.

62 L. Dačanin, S. R. Lukić, D. M. Petrović, M. Nikolić and M. D. Dramićanin, *Phys. B*, 2011, **406**, 2319–2322.

63 R. Y. Yang, Y. M. Peng, H. L. Lai, C. J. Chu, B. Chiou and Y. K. Su, *Opt. Mater.*, 2013, **35**, 1719–1723.

64 R. E. M. Khaidir, Y. W. Fen, M. H. M. Zaid, K. A. Matori, N. A. S. Omar, M. F. Anuar, S. A. A. Wahab and A. Z. K. Azman, *Optik*, 2019, **182**, 486–495.

65 M. N. Bessadok, W. Ahmed, H. Jeidi, C. Bouzidi, N. Ihzaz, C. Barthou and L. El Mir, *Phys. B*, 2022, **624**, 413441.

66 J. El Ghoul and L. El Mir, *J. Mater. Sci.:Mater. Electron.*, 2015, **26**, 3550–3557.

67 A. Apostoluk, Y. Zhu, P. Gautier, A. Valette, J. M. Bluet, T. Cornier, B. Masenelli and S. Daniele, *Materials*, 2023, **16**, 5400.

68 S. Mrabet, N. Ihzaz, M. N. Bessadok, C. Vázquez-Vázquez, M. Alshammari and L. El Mir, *J. Inorg. Organomet. Polym. Mater.*, 2024, **34**, 2064–2073.

69 L. El Mir, K. Omri and J. El Ghoul, *Superlattices Microstruct.*, 2015, **85**, 180–184.

70 K. Nigoghossian, Y. Messaddeq, D. Boudreau and S. J. L. Ribeiro, *ACS Omega*, 2017, **2**, 2065–2071.

71 R. G. Geitenbeek, P. T. Prins, W. Albrecht, A. Van Blaaderen, B. M. Weckhuysen and A. Meijerink, *J. Phys. Chem. C*, 2017, **121**, 3503–3510.

72 O. A. Savchuk, J. J. Carvajal, C. Cascales, M. Aguiló and F. Díaz, *ACS Appl. Mater. Interfaces*, 2016, **8**, 7266–7273.

73 Y. Sun, W. Chen, S. Liu, S. Yan, S. Zhang, L. Huang and Z. Zheng, *J. Solid State Chem.*, 2021, **301**, 122296.

74 I. M. Alibe, K. A. Matori, H. A. A. Sidek, Y. Yaakob, U. Rashid, A. M. Alibe, M. H. M. Zaid and M. Z. A. Khiri, *Molecules*, 2018, **23**, 1–18.

75 L. Skuja, N. Ollier and K. Kajihara, *Radiat. Meas.*, 2020, **135**, 106373.

76 T. Garmysheva, A. I. Nepomnyashchikh, A. Shalaev, E. Kaneva, A. Paklin, K. Chernenko, A. P. Kozlova, V. Pankratov and R. Shendrik, *J. Non-Cryst. Solids*, 2022, **575**, 121199.

77 I. Parkhomenko, L. Vlasukova, F. Komarov, M. Makhavikou, O. Milchanin, E. Wendler, M. Zapf and C. Ronning, *J. Phys. D Appl. Phys.*, 2021, **54**, 265104.

78 A. P. Baraban, S. N. Samarin, V. A. Prokofiev, V. A. Dmitriev, A. A. Selivanov and Y. Petrov, *J. Lumin.*, 2019, **205**, 102–108.

79 M. Runowski, N. Stopikowska, D. Szeremeta, S. Goderski, M. Skwierczyńska and S. Lis, *ACS Appl. Mater. Interfaces*, 2019, **11**, 13389–13396.

80 C. D. S. Brites, K. Fiaczyk, J. F. C. B. Ramalho, M. Sójka, L. D. Carlos and E. Zych, *Adv. Opt. Mater.*, 2018, **6**, 1–5.

81 W. Wang, L. Li, J. Xie, Q. Cao, Y. Li, X. Shen and Y. Pan, *J. Lumin.*, 2024, **266**, 120289.

82 R. Wei, F. Lu, L. Wang, F. Hu, X. Tian and H. Guo, *J. Mater. Chem. C*, 2022, **10**, 9492–9498.

83 J. Kong, Y. Wang, W. Tong, L. Li, Y. Xu, N. Chen and N. Liu, *J. Alloys Compd.*, 2024, **983**, 173936.

84 S. Das, S. Som, C. Y. Yang, S. Chavhan and C. H. Lu, *Sci. Rep.*, 2016, **6**, 1–13.

85 M. Zhu, Q. Ma and N. Guo, *Spectrochim. Acta, Part A*, 2022, **271**, 120922.

86 H. Zhou, N. Guo, Q. Liang, Y. Ding, Y. Pan, Y. Song, R. Ouyang, Y. Miao and B. Shao, *Ceram. Int.*, 2019, **45**, 16651–16657.

87 P. Yang, L. Li, Y. Deng, Y. Wang, S. Jiang, X. Luo, G. Xiang, Y. Lu and X. Zhou, *Dalton Trans.*, 2019, **48**, 10824–10833.

88 I. E. Kolesnikov, D. V. Mamonova, M. A. Kurochkin, E. Y. Kolesnikov and E. Lähderanta, *ACS Appl. Nano Mater.*, 2021, **4**, 1959–1966.

89 P. Du, X. Sun, Q. Zhu and J. G. Li, *Scr. Mater.*, 2020, **185**, 140–145.